Simultaneous Control of Multiple MEMS Microrobots

Bruce R. Donald[1,2,6], Christopher G. Levey[3], Igor Paprotny[1,4], and Daniela Rus[5]

[1] Department of Computer Science, Duke University, Durham, NC, USA.
[2] Department of Biochemistry, Duke University Medical Center, Durham, NC, USA.
[3] Thayer School of Engineering, Dartmouth College, Hanover, NH, USA.
[4] Department of Computer Science, Dartmouth College, Hanover, NH, USA.
[5] Department of EECS, MIT, Cambridge, MA, USA.

Abstract: We present control algorithms that implement a novel planar microassembly scheme using groups of stress-engineered microrobots controlled through a single global control signal. The global control signal couples the motion of the devices, causing the system to be highly underactuated. Despite the high degree of underactuation, it is desirable that each robot be independently maneuverable. By exploiting differences in the designs and the resulting electromechanical interaction with the control signal, the behavior of the individual robots can be differentiated. We harness this differentiation by designing the control signal such that some devices remain confined in small circular orbits (limit cycles), while the non-orbiting robots perform work by making progress towards the goal. The control signal is designed to minimize the number of independent control voltage levels that are used for independent control, allowing us to maximize the number of simultaneously controllable devices.

Our algorithms were tested on systems of fabricated untethered stress-engineered MEMS microrobots. The robots are 240–280 μm $\times$ 60 μm $\times$ 7–20 μm in size and are controlled in parallel (simultaneously) within the same operating environment. We demonstrated the feasibility of our control algorithms by accurately assembling 5 different types of planar microstructures.

1 Introduction

The operation of multiple untethered microrobotic devices have many potential applications in medicine, surveillance, and assembly [13]. In this work we use the term *microrobot* to denote an untethered robot that fits strictly within a 1 mm^3 volume.

In [6], we presented a globally controllable 240 μm $\times$ 60 μm $\times$ 10 μm mobile stress-engineered MEMS microrobot. A scanning-electron micrograph of a stress-engineered MEMS microrobot, and an optical micrograph of four microrobots during an assembly experiment, are shown in Figure 1. The robot has a *steering arm* (Fig. 1a(i)), and operates on a planar substrate (its *operating environment*), which couples an external control and power delivery signal to the device regardless of its pose. Simultaneous control of multiple microrobots within a single operating environment is desirable, but presents a significant challenge when only a single, global

[6] Corresponding author: brd+wafr08@cs.duke.edu

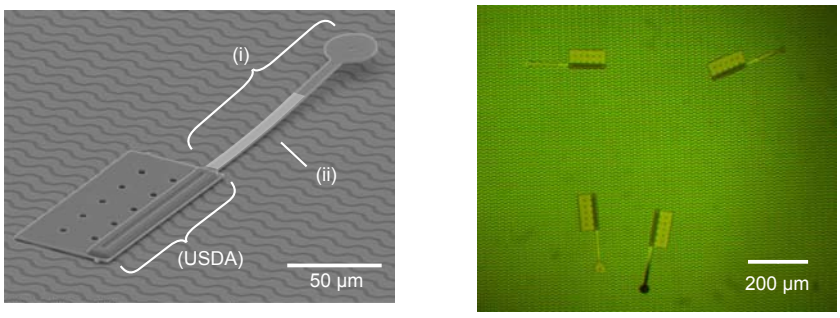

(a) (b)

Fig. 1. Scanning-electron micrograph of a stress-engineered MEMS microrobot (a), and optical micrograph of four microrobots (b). **a:** The microrobot consists of an untethered scratch-drive actuator (USDA) that provides forward motion, and a curved steering-arm actuator (i) that determines whether the robot moves in straight-line motion or turns. A lithographically-patterned chrome-layer defines the curvature of the steering arm (ii). **b:** Four different stress-engineered microrobots on their operating environment. The robots are differentiated by the design of their steering-arm actuators.

control signal can be used to control all the devices: the resulting system is highly underactuated.

We show that designing microrobots with different steering arms that respond to different voltages allows us to independently maneuver multiple microrobots. Each steering arm has two *transition voltages* (voltage levels at which the steering arm is either pulled down or released from the substrate). We show that it is sufficient that each steering arm has a unique transition voltage pair, i.e. the combination of both transition voltages is unique. Details of fabrication, designs and testing were reported in [8]. In this work, we present the theory for designing the control signal to enable simultaneous control of multiple microrobots for microassembly. Enabling our control algorithms are new theorems that minimize the control bandwidth requirements. These theorems were essential for controlling multiple untethered microrobots to move and assemble independently, and are not covered in [8].

We underscore that at the micro- and nano-scale it is difficult to build and test untethered robotic devices, let alone make these devices perform useful tasks. We had to resort to engineering and control designs that could likely be obviated at the macroscopic scale, but were necessary at micro-scale. Every theoretical idea in this paper has been experimentally tested, at least to proof-of-principle. Our algorithms cope with the control couplings and high level of underactuation present in our microrobot systems. At the macroscale these might also be engineered out, but at the microscale they are a consequence of Global Control, Selective Response (GCSR) [5], and GCSR is presently the only scalable control paradigm for multiple microrobots.

2 Related Work

Small, often completely autonomous mobile robotic devices, with size on the order of centimeters [12] are called *miniature robots*. Miniature robots containing microfabricated components [11] are called MEMS robots. The components of MEMS robots are often manufactured separately and then assembled to form complete systems. The size of such MEMS robots ranges from hundreds of micrometers to several centimeters. In [6, 8] and this paper, we use the term *microrobot* to denote mobile untethered MEMS robots with their dimensions strictly confined within a 1 mm^3 cube. Other microrobotic systems include a magnetic micro-needle that is actuated using magnetic fields [16].

Microassembly is one potential application for cooperating microrobotic systems. Currently, the assembly of micro-components is performed either using serial robotic manipulators with micro-scaled end-effectors [3], using a distributed manipulation approach, [1, 14], or through parallel but less controllable self-assembly (SA) [15]. In contrast with SA, our microassembly scheme relies on intersecting trajectories, rather than component affinity, to promote structure aggregation. The concept of selective response of individual units to a global, broadcasted, control signal (Global Control, Selective Response (GCSR) [5]) is common in micro- or nanoscale biological systems. Bretl [2] presented a related theoretical motion planning approach for systems of robots with limited controllability, showing that even simple devices controlled through a global signal can perform useful tasks.

3 Stress-engineered MEMS Microrobot

All the control and assembly algorithms presented in this paper are implemented using groups of parallel-actuated stress-engineered MEMS microrororobots [6]. A stress-engineered microrobot has two actuated internal degrees of freedom (DOF); an untethered scratch-drive actuator (USDA) [7] that provides forward locomotion, and a steering-arm actuator that determines whether the robot moves in a straight-line or turns. The steering-arm consists of a cantilever beam with a circular pad and a .75–1.2 μm deep dimple. The cantilever beam is curved (out-of-plane) using a stress-engineering process [8], which determines the deflection of the steering arm. The microrobot operates on fields of zirconia-insulated interdigitated electrodes. When a voltage is applied across these electrodes, the electrodes and the conductive microrobot chassis form a capacitive circuit inducing an electric potential on the microrobot body. This voltage (waveform) is varied over time to provide power to the untethered scratch-drive actuator and to control the state of the steering-arm. This waveform is called the *control waveform*. Figure 2(a) illustrates one cycle of the control waveform. The waveform is divided into a *control cycle*, containing one or more *control pulses* ($V_{a,j}$), that sets the state of the steering-arm actuator, and a *power-delivery cycle* that provides power to the scratch-drive actuator. For a single robot, a specific control waveform, defined through the voltage triple ($V_{a,1}$, V_b, V_s), is called a

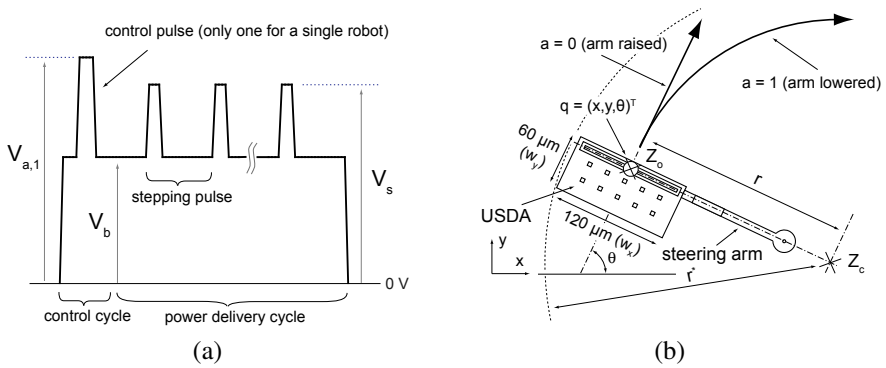

Fig. 2. The control and power delivery waveform for a single stress-engineered MEMS microrobot (a), and kinematics of the stress-engineered MEMS microrobot (b).

control primitive; one control primitive causes the robot to turn, while another causes it to move in a straight line.

Similar to an electrostatic cantilever beam, the steering arm of the stress-engineered MEMS microrobot has two distinct voltage-levels at which it abruptly changes state. These voltages are called the *transition voltages*. While clearly the state of our microrobot includes the state of the steering arm and the state of the scratch-drive actuator, for the purpose of this section it suffices to consider only the states of the steering-arm actuators, which we call the robots' *control states*. Consequently, a single actuated stress-engineered microrobot can be in one of only two control states; the steering-arm can be either raised (0) or lowered (1). When the voltage supplied to the robot reaches the steering-arm's *snap-down* transition voltage (V_d), the arm is pulled into contact with the substrate. When the voltage is reduced past the *release* transition voltage (V_u), the arm is released from the substrate. The transition voltages are a function of the design of the individual steering-arm actuators: for example, smaller air gaps or larger steering pads reduce both V_u and V_d. Microrobots with identical steering-arms are classified as belonging to the same *microrobot species*. The difference between the snap-down and release voltage of a steering-arm is called the *hysteresis gap*.

The kinematics of our robot is illustrated on Fig. 2(b). The configuration of the robot is given by the vector $q = (x, y, \theta)^T$ in configuration space (C-space). The configuration of the robot is measured at the point Z_o in the middle of its bushing. The robot moves like a Dubins car that can turn in one direction only. The velocity of the robot is $\dot{q} = v\left(\sin\theta, \cos\theta, \frac{ah}{r}\right)^T$, where $h \in \{-1, 1\}$ and denotes whether the steering arm is on the right or the left side, v is the velocity of the scratch-drive actuator, r is the turning radius and $a \in \{0, 1\}$ is the state of the steering arm (0 = up, 1 = down). The velocity v can be varied by changing the frequency of the stepping pulses, however for the remainder of this paper we will consider v to be a positive constant (positive because the robot can not back up). It follows that the robot is not *small-time locally controllable* (STLC).

4 STRING Theory: Control Signal Design for Parallel Actuation

Multiple microrobots operating simultaneously within the same environment receive the same, single, global control signal. Here we show how to design the control signal, constructing a set of control primitives that allows us to independently maneuver multiple microrobots when implementing microassembly.

Suppose we have a set of m control primitives that can be applied through the operating environment to control a set of n microrobots. A mapping between the control primitives and the motion of the individual devices is expressed through a *control matrix* M of size $(n \times m)$, where each entry (i, j) contains the control state of microrobot j during the application of the control primitive i. The control matrix describes the coupling of the microrobot motion as a function of the control signal, linking the electromechanical functionality of the steering-arms with the application of the control primitives. An example of the control matrix is shown in Eq. (3) on p. 8. Our control strategies (described in sec. 5) require that the control matrix is structured such that the robots progressively start turning as the control primitives with higher index i are applied. We prove that such a control matrix can be constructed with the smallest number of independent voltage levels in the control signal necessary to achieve independent control, allowing us to maximize the number of simultaneously controllable microrobots.

For a system of n microrobots, let $V_{d,i}$ and $V_{u,i}$ denote the snap-down and release voltages of microrobot i. Let V_Ω be the breakdown voltage of the operating environment, V_{flx} be the minimum voltage at which the backplate of the USDA generates enough flexure to produce a forward step of the scratch-drive actuator, and V_{rel} be the maximum voltage at which the backplate of the USDA relaxes, allowing it to take a step forward (each stepping pulse must cycle through V_{flx} and V_{rel} in order to supply power to the USDA). The snap-down and release voltages of each device must satisfy to the following constraints:

1. $V_{d,i} < V_\Omega$: snap-down voltage cannot exceed the break-down voltage of the operating environment.
2. $V_{d,i} > V_{u,i}$: dictated by the electromechanics of cantilever beams.
3. $V_{rel} > V_{u,i}$ for all i : ensures the microrobot can receive power during all the control states.
4. $V_{flx} \leq \overset{min}{i} (V_{d,i})$: Ensures that the USDA flexes sufficiently to produce forward motion during the power delivery cycle.

The *control voltage bandwidth* ξ of a microrobot system is the number of independent electromechanically-addressable transition voltage levels that can be used for control. ξ depends on four parameters: the break-down voltage of the operating environment, V_Ω, the inherent variability of the power coupling between the robot and the underlying substrate, the precision of the fabrication process, and the minimum range of voltages required to reliably power the USDA, V_{SDA} ($V_{SDA} = V_{flx} - V_{rel}$). The variability in the power coupling causes deviations in the potential induced between the steering arm and the substrate, while inaccuracies in the fabrication process cause deviations in the transition voltages of the steering arms.

Let δ_v be the maximum deviation of the transition voltage manifested during the microrobot operation, determined by these two parameters. We define two transition voltages to be *significantly independent* if they are separated by at least $2\delta_v$. Note that, although in general, $V_{SDA} = V_{flx} - V_{rel}$, it is possible for the stepping pulse to overlap with the lowest snap-down voltage, $\min_{i \in Z_n} V_{d,i}$. Consequently, we define V'_{SDA} as the *additional* control voltage bandwidth that is required by the power delivery cycle to ensure reliable actuation of the USDA, as follows:

$$V'_{SDA} = \begin{cases} 0, & \text{if } V_{flx} - V_{rel} \leq 2\delta_v, \\ V_{flx} - V_{rel} - 2\delta_v, & \text{otherwise.} \end{cases} \tag{1}$$

The control voltage bandwidth of a microrobot system is then $\xi = \left\lfloor \frac{V_Q - V'_{SDA}}{2\delta_v} \right\rfloor$, assuming V_{flx} and V_{rel} can vary by at least $2\delta_v$ (otherwise $\xi = \left\lfloor \frac{V_{rel}}{2\delta_v} \right\rfloor + \left\lfloor \frac{V_Q - V_{flx}}{2\delta_v} \right\rfloor$). How much of ξ is actually used to control the microrobotic system is related to the number of accessible control states of the steering arm actuators. Define the *control voltage bandwidth requirement*, ξ_n, of a n-microrobot system as the number of independent voltage levels necessary to achieve independent control during our microassembly application. Clearly it must hold that $\xi_n \leq \xi$. In general, a microrobotic system with fewer accessible control states has a lower control voltage bandwidth requirement. More specifically, the accessibility of the control states depends on the relation between the hysteresis gaps of the individual robots.

Consider a system of two microrobots, D_1 and D_2, with steering arms that have *Nested Hysteresis Gaps* (NHG) (first proposed in [6]). Fig. 3(a) shows the relation between the transition voltages for such a system. The snap-down and release voltages are shown as circles and rectangles, respectively. Without loss of generality, we consider only significantly independent voltage levels of the control signal (labeled as V_α-V_δ on Fig. 3). Fig. 3(b) shows the programming cycles for the four control primitives that access the four control states (11), (10), (01) and (00) (we assume $V_b = V_{rel}$). More generally, we classify the system of n steering arms, sorted according to ascending $V_{d,i}$, as having NHG when $(V_{d,i} + 2\delta_v < V_{d,j})$ and $(V_{u,i} - 2\delta_v > V_{u,j})$, for all $i < j$. NHG systems can access all 2^n control states. However each device requires two unique control voltage levels, and so the control voltage bandwidth requirement of this system is $\xi_n = 2n$.

NHG are sufficient but not necessary, to control multiple devices during assembly. Consider a two-robot system where the hysteresis gaps of the robots are not nested, as shown in Fig. 4(a). In this particular system, only three control states are electromechanically accessible. The control cycles (control pulses only) that access all three control states, (00), (10) and (11), are shown in Fig. 4(b). Control state (01) can not be accessed, because pulling down the steering-arm of D_2 also pulls down the steering-arm of D_1, and the steering-arm of D_1 can not be released without also releasing the arm of D_2.

In general, an n-microrobotic system, first sorted according to ascending values of V_d, and then sorted according to ascending values of V_u, has non-nested hysteresis gaps if $(V_{d,i} \leq V_{d,j})$ and $(V_{u,i} \leq V_{u,j})$, for all $i < j$. However, in the case when $|V_{d,i} -$

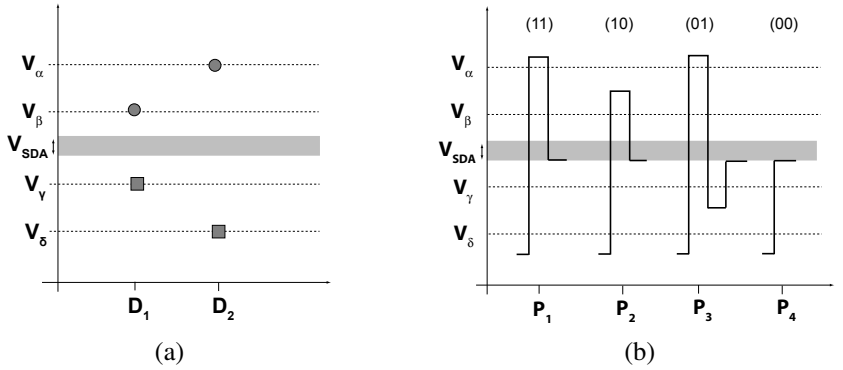

(a) (b)

Fig. 3. Transition voltages for a system of two microrobots with nested hysteresis gaps (NHG) (**a**), and the control cycles for the four control primitives that access all control states for the system (**b**).

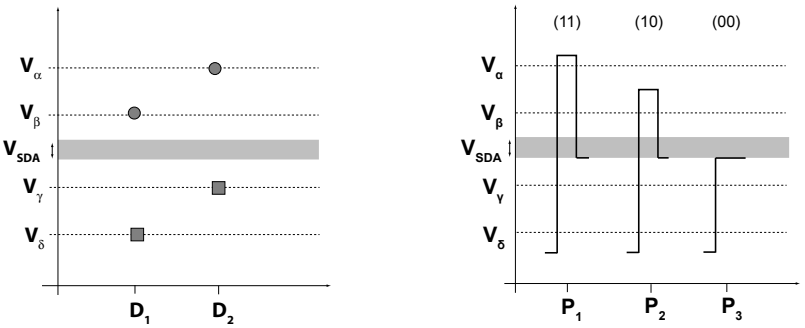

(a) (b)

Fig. 4. Transition voltages for a system of two microrobots with non-nesting hysteresis gaps (**a**), and the control cycles for the control primitives that access three of the control states for the system.

$V_{d,j}| < 2\delta_v$ and $|V_{u,i} - V_{u,j}| < 2\delta_v$, the behavior of robots i and j is indistinguishable, and such two devices cannot be controlled independently. We call such two robots a *degenerate pair*. Let a *STRIctly Non-nested hysteresis Gaps* (STRING) system be a non-nested hysteresis gap system with no degenerate pairs of devices.

Lemma 1. *An n-robot STRING system has exactly* $n + 1$ *accessible control states.*

The complete proof of Lemma 1 is provided in Supplementary Material (**SM**) **Section 1** available online in Ref. [10]. We now construct the control primitives and corresponding control matrix that can access the $n + 1$ control states of a n-robot STRING system. The ordering of the robots is determined by the transition voltages of the steering arms, i.e., the robots must be primarily sorted according to increasing order of $V_{u,i}$ and secondarily sorted according to increasing order of $V_{d,i}$.

We construct the control primitive P_j such that it snaps down the arms of devices D_i for $i \leq j$, and releases the arms of devices D_i for all $i > j$. P_j is defined by a control cycle containing two control pulses, $P_j = (V_{a,1}, V_{a,2})$, assume $V_b = V_{rel}$ and $V_s = V_{flx} \leq V_{d,1}$. Consider the STRING system shown on Fig. 5(a), where $V_\alpha, \cdots, V_\epsilon$ represent significantly independent control voltage levels. We define P_j as:

$$P_j = \begin{cases} (V_0, V_0), & \text{if } j = 0; \\ \left(V_{d,j}, V_{u,j+}\right), & \text{if } j \in Z_{n-1}; \\ (V_{d,n}, V_{d,n}), & \text{if } j = n, \end{cases} \tag{2}$$

where $V_{u,j+} = V_{u,j} + 2\delta_v$. In practice, $V_{u,j+}$ is the next significantly independent release voltage above $V_{u,j}$. Also, note that in order for $V_{d,j}$ to cause *reliable* snap down, it must be δ_v *above* the designed (nominal) $V_{d,j}$ level. Correspondingly, $V_{u,j}$ must be δ_v *below* the designed (nominal) $V_{u,j}$ level to ensure reliable steering arm release.

The first control pulse ($V_{a,1}$) snaps down the steering arms of all the devices D_i, $i \in Z_j$, as well as any devices D_k, $k > j$ with $V_{d,k} = V_{d,j}$. The second control pulse ($V_{a,2}$) releases all the devices D_k, $k > j$ that were snapped down by the first control pulse, because in the case when $V_{d,k} = V_{d,j}$, it must hold that $V_{u,j} < V_{u,j+} \leq V_{u,k}$. An example control cycle is also shown in Fig. 5(a).

The $n+1$ control primitives generated by P_j form a $(n+1) \times n$ control matrix M. An example of such control matrix for four devices is:

$$M = \begin{pmatrix} 0 & 0 & 0 & 0 \\ 1 & 0 & 0 & 0 \\ 1 & 1 & 0 & 0 \\ 1 & 1 & 1 & 0 \\ 1 & 1 & 1 & 1 \end{pmatrix}. \tag{3}$$

We refer to M as the *STRING control matrix*, the $n+1$ control primitives contained in M as the *STRING control primitives*, and the $n+1$ control states accessible using these control primitives as the *STRING control states*. Note that because adding a new control state to a STRING system requires the addition of another independent voltage level (per Lemma 1), the control bandwidth requirement for a STRING system is $\xi_n = n + 1$.

Lemma 2. *Any stress-engineered n-microrobotic system with no degenerate pairs of robots can be sorted such that all* $n+1$ *STRING control states are accessible.*

Proof. By construction. Consider a microrobot system with k independent snap-down voltages, and ℓ independent release voltages. Assuming no degenerate pairs of devices, it follows that $n \leq k\ell$. In the case when $n = k\ell$, the n steering arms encode all the possible $k\ell$ combinations of snap-down and release voltages. We call such system for *electromechanically saturated* (ESat). We can enumerate the hysteresis gaps for an ESat system given both k and ℓ. Consider an ESat system, sorted primarily according to increasing release voltage $V_{u,i}$ and secondarily sorted according

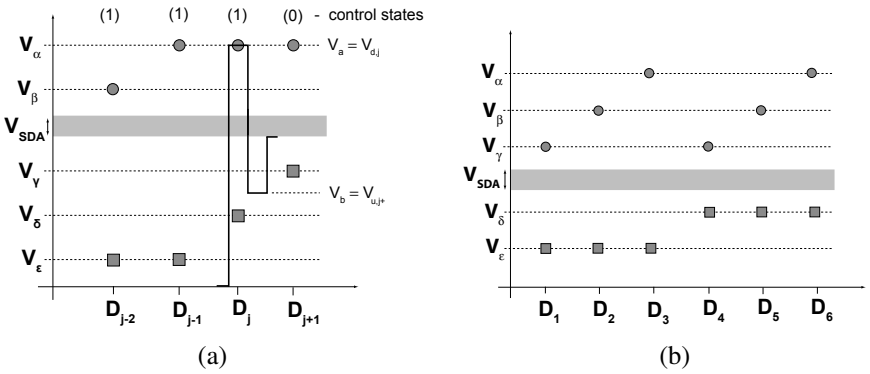

Fig. 5. Construction of a STRING control matrix (a), An example of an ESat system with $k = 3$ and $l = 2$ (b).

to increasing snap-down voltage $V_{d,i}$. Fig. 5(b) shows such system when $k = 3$ and $l = 2$. Note that sorting ensures a monotonic increase of $V_{u,i}$ with increasing index i. For such an order, there exists a recursive formula, shown in Eq. (4), that generates all $n + 1$ STRING control primitives. The control cycle for each control primitive defined by Eq. (4) contains a sequence of up to $2n$ control pulses (in contrast with 2 control pulses in Eq. (2)). Again, we assume $V_b = V_{rel}$ and $V_s = V_{flx} \leq V_{d,1}$.

$$P_j = \begin{cases} (V_0, V_0), & \text{if } j = 0; \\ \left(P_{j-1}, V_{d,j}, V_{u,j+}\right), & \text{if } j \in Z_n. \end{cases} \tag{4}$$

P_j generates $n + 1$ control primitives that form a STRING control matrix, by causing devices D_i ($i \leq j$) to be in state 1, while robots D_i ($i > j$) are in state 0. Consider the base case P_0, where all D_j, ($j \in Z_n$) is in state 0. We make the inductive argument that after application of the recursive part of P_j, P_{j-1}, all $D_1, \cdots, D_{j-1}$ robots are in control state 1. It is clear that $V_{d,j}, V_{u,j+}$, ($j \in Z_n$), will snap down D_j. The $V_{u,i}$- then $V_{d,i}$-sorting implies that, for a device D_k, $k > j$, only two case are possible with respect to its transition voltages: (a) $V_{d,j} < V_{d,k}$ (e.g. $j = 2$ and $k = 3$ in Fig. 5(b)), or (b) $V_{u,j} < V_{u,j+} \leq V_{u,k}$ (e.g. $j = 3$ and $k = 5$ in Fig. 5(b)). It is clear that in case (a), $V_{d,j}$ sets D_j to state 1, while D_k, $k > j$ is in state 0. The sorting ensures that any previously applied control primitive P_i, $i < j$ with $V_{a,1} \geq V_{d,k}$ (which also inadvertently snaps down the arm of D_k) must have have been followed by a control pulse $V_{a,2} \leq V_{u,k} - 2\delta_v$ (which would release the arm of D_k). In case (b), $V_{u,j+}$ releases any devices D_k, $k > j$. □

Note that because the devices are sorted according to $V_{i,u}$ and $V_{d,i}$, Eq. (4) also holds for any microrobotic system, even one that is not ESat.

Theorem 1. *A system of n STRING microrobots contains the minimum number (n+1) of electromechanically accessible control states of any stress-engineered microrobot system without degeneracy.*

Proof. Per Lemma 1; an n-microrobot STRING system has exactly $n + 1$ accessible control control states, and by Lemma 2, any n stress-engineered microrobotic system without degenerate pairs of robots contains at least $n + 1$ control states. □

Theorem 2. *An algorithm that solves the gross motion planning problem (i.e. finds the control sequence S) for a STRING system can be applied to solve the gross motion planning problem for any non-degenerate system of stress-engineered microrobots.*

Proof. A consequence of Lemma 2; a STRING control matrix can be constructed for any n-stress-engineered microrobotic system. □

Theorem 2 allows us to further reduce the control bandwidth requirements for a microrobotic system. The control voltage bandwidth requirement for a microrobot system with k independent snap-down voltage levels and ℓ independent release voltage levels is $\xi_n = k+\ell$. In an ESat system, $n = k\ell$. It follows that n is maximized when $\ell = k = \xi_n/2$, and $n = \xi_n^2/4$. We call such system *symmetric electromechanically saturated*, or SESat. As a consequence, the control bandwidth requirement for an ESat system is $\xi_n \geq 2\lceil \sqrt{n} \rceil$, while it is $\xi_n = 2\lceil \sqrt{n} \rceil$ for an SESat system. It follows that an SESat system maximizes the number of simultaneously controllable microrobots.

5 STRING Parallel Control for Microroassembly

We now use the structure of the STRING matrix M to decouple the motion of the individual robots by reducing the problem of controlling n microrobots in parallel to the problem of controlling only two robots in parallel, followed by sequential control of single devices. We can perform this reduction whenever M has the form of a STRING control matrix by constraining some robots to orbit along limit cycles without making progress towards the goal. Note that our planning algorithms are not fully general and require a minimum separation between the orbiting robots.

The assembly is performed in $n-1$ steps. Fig. 6(a) and (b) show the assembly for a system of $n = 3$ microrobots assembling the shape $\mathcal{G}_2$ (from Fig. 9). The STRING control matrix M for this system is shown on Eq. (3) p. 8. Further details of the reduction are provided in **SM** [10] **Section 2**.

5.1 Microassembly Step 1

The two microrobots with the highest index, D_{n-1} and D_n are maneuvered to assemble an initial stable shape, $\mathcal{G}_1$. Only control primitives P_{n-2}, P_{n-1} and P_n are used to control D_{n-1} and D_n. P_{n-2}, P_{n-1} and P_n cause only turning motion in robots D_i, ($i < n-1$, e.g. robot D_1 in Fig. 6(a)), and consequently these robots remain in circular orbits. The assembly of $\mathcal{G}_1$ takes place in two stages, because even though both D_{n-1} and D_n move simultaneously, error correction is only performed on a single microrobot at any given time.

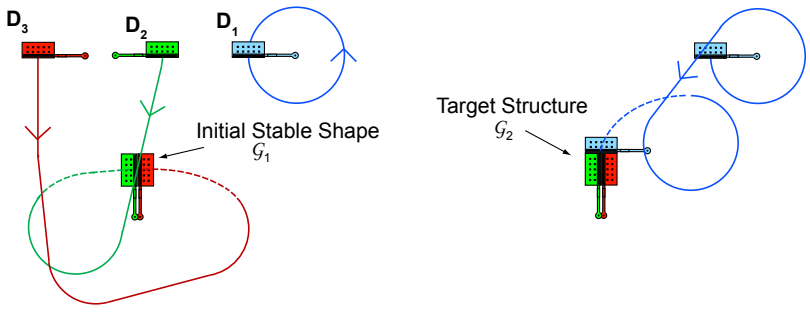

(a) (b)

Fig. 6. Example assembly of three microrobots in two steps. **a:** Step 1, the assembly of the initial stable shape. **b:** Step 2, docking of D_1 to form the target shape.

5.2 Microassembly Step $2, \cdots, n-1$

A single robot, D_i, is maneuvered to dock with the assembling shape (See Fig. 6(b)). Only control primitives P_i and P_{i-1} are used to maneuver D_i, causing the devices D_j, $(j < i)$, to follow circular orbits. Because the target shape ($\mathcal{G}_k$ out of a set of p available target shapes, $\mathcal{G} = \{\mathcal{G}_1, \mathcal{G}_2, \cdots, \mathcal{G}_P\}$) is assembled in the descending order of the device index i, the devices D_j, $(j > i)$ are immobilized by compliance within the assembling shape.

5.3 EDR-based Control

We used the theory of Error Detection and Recovery (EDR) [4] to construct control strategies that allow us to reliably maneuver the microrobots to target regions in the presence of control error. Our control strategies are based on progressive execution and replanning of the microrobot trajectories during each of the steps described above. However, in order to increase the precision of the assembly, we switch to a fine-motion control strategy as the robots approach their docking configurations (the dashed trajectories in Fig. 6). The fine-motion trajectory is based on interpolated turning, and allows us to sacrifice precise control of the incident angle for the docking robot in favor of precise control of its docking location. The accumulating error in rotation is later reduced using compliance. Details regarding the control strategies are provided in **SM** [10] **Section 3** for the interested reviewer.

6 Experimental Results

The control strategies presented in this paper have been tested experimentally on groups of fabricated stress-engineered micrororobots. This section uses experimental data that has been previously reported in [8], but describes how this data validates the algorithms above, and gives the explicit construction of the control matrices necessary to replicate the results.

6.1 Fabrication of STRING Microrobots

We fabricated 15 microrobots classified into five microrobot *species*. The microrobot species are differentiated through the designs of their steering arm actuators. Fig. 7 shows a scanning-electron micrograph of a microrobot from each species. The species are designed such that multiple copies can be reproducibly fabricated despite the inherent variability of our fabrication process.

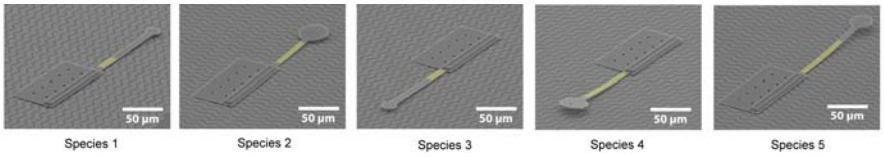

Fig. 7. *Reprinted with permission from [8].* Scanning-electron micrographs of the five microrobot species used to implement microassembly. Yellow color is used to highlight the areas of the steering-arms covered by the chrome layer.

The steering-arm designs were determined based on closed-form equations [6], finite-element analysis and empirical data, such that the transition voltage, ($V_{d,i}$ and $V_{u,i}$), for all the robots are reproducibly confined to the ranges shown in Fig. 8(a). Snap-down voltages ($V_{d,i}$) are marked by circles, while the rectangles denote the release voltages ($V_{u,i}$). The ranges are marked by a vertical bar, with two dots signifying that the lower or upper bound is not fixed or measured. Groups of robots from species 1,3,4,5 and 2,3,4,5 form STRING systems, while species 1 and 2 form a degenerate pair. The exact parameters of the steering-arms defining all five species are described in [8]. The waveforms (control pulse and three power delivery pulses only) of the five control primitives used to control the four-robot STRING groups are show in Fig. 8(b). Average V_a, V_b and V_s voltage levels are shown. The actual voltage-levels used to control the individual groups of microrobots could vary by up to ± 10 V.

6.2 Microassembly

We applied the control algorithms to groups of four STRING microbots, generating a total of 14 planar structures. The assembled structures belong to five types of target shapes, labeled $\mathcal{G}_1 - \mathcal{G}_5$. Optical micrographs of microstructures for each type of target shape are shown on Fig. 9.

The robots were operated on a 2 mm^2 environment, and their position was registered using a digital video-camera attached to an optical microscope with a 6.7 × objective lens. The position of the devices was extracted with a precision of ± 2.1 μm. The humidity was kept below 4% RH using a continuous stream of dry nitrogen during the experiments. The waveforms for the control primitives were produced using an Agilent 33120A arbitrary waveform generator, and amplified with a Trek

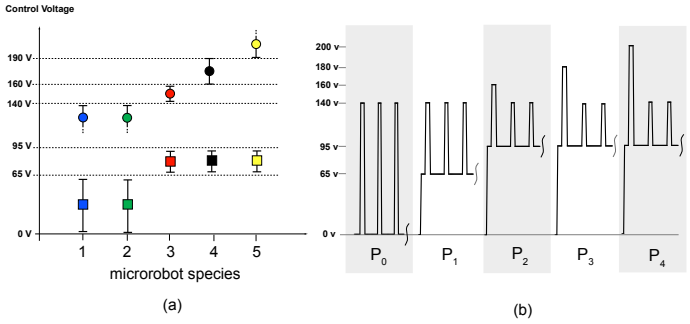

Fig. 8. Transition voltage ranges (a) and corresponding control primitives (b) used to control the five microrobot species.

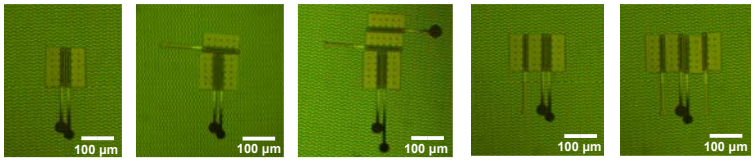

Fig. 9. *Reprinted with permission from [8].* Optical micrographs of five types of target shapes assembled using our microrobots.

PZD700-1 high-voltage power amplifier with a gain of 200. The duration of the individual control primitives was entered manually into the waveform generator.

Table 1 shows the average match (portion of the target structure covered by the assembled shape) for the five assembled shapes, $\mathcal{G}_1 - \mathcal{G}_5$. The assembly experiments were conducted starting from two different classes of initial configurations: $\mathcal{R}_1$ – robots are arranged along the corners of a rectangle with sides 1 by 0.9 mm, all devices oriented along the y-axis (see Fig. 10(a) for a representative example), and $\mathcal{R}_2$ – robots are arranged in a line with average separation of 360 μm, and with variable orientation. The initial position of the microrobots was set using batch-transfer structures called *transfer-frames* [8] and microprobes. We used common geometric shapes (a line and a rectangle) to demonstrate the ability to achieve successful assembly from arbitrary different initial configurations.

The results in Table 1 do not include completely failed assemblies. We recorded a 11% failure rate during the consecutive assembly of nine structures over the course of three assembly experiments. This reflects that the assembly of one of the nine structures failed due to the loss of stability of an intermediate structure, which was attributed to an initial unfortunate misalignment between the microrobots forming the intermediate assembly. Fig. 10 illustrates a representative assembly experiment.

Table 1. Precision of Microassembly.

	Goal Configurations					
Initial Configurations	$\mathcal{G}_1$	$\mathcal{G}_2$	$\mathcal{G}_3$	$\mathcal{G}_4$	$\mathcal{G}_5$	**Average**
$\mathcal{R}_1$	96 ± 4% (3 runs)	98 ± 3% (2 runs)	96 ± 2% (2 runs)	96% (1 run)	93% (1 run)	96 ± 3% (3 runs)
$\mathcal{R}_2$	99 ± 2% (2 runs)	98% (1 run)	93% (1 run)	89% (1 run)	na	95 ± 4% (2 runs)
Average	97 ± 3% (5 runs)	98 ± 2% (3 runs)	95 ± 2% (3 runs)	93 ± 5% (2 runs)	93% (1 run)	96 ± 3% (5 runs)

In this experiment, the target shape $\mathcal{G}_5$ is generated via the assembly of $\mathcal{G}_1$ and $\mathcal{G}_4$. The experiment terminated when all four microrobots were successfully incorporated in the assembled structure. A movie of this assembly experiment is available online at [9].

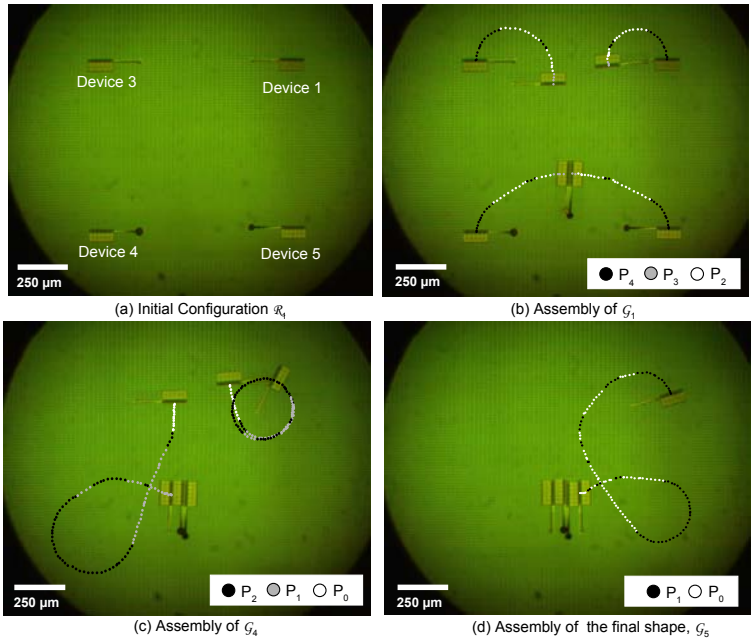

(a) Initial Configuration $\mathcal{R}_1$ (b) Assembly of $\mathcal{G}_1$

(c) Assembly of $\mathcal{G}_4$ (d) Assembly of the final shape, $\mathcal{G}_5$

Fig. 10. *Reprinted with permission from [8].* Composite optical micrograph of experimental assembly-data using devices from species 1,3,4 and 5. The devices are labeled according to the number of their respective species.

7 Conclusions

We presented novel control algorithms for implementing planar microassembly using groups of stress-engineered microrobots. The experimental data, reprinted from [8], indicates the feasibility of our algorithms, and represents the first implementation of a multi-microrobotic system. This work presents the planning and control challenges to achieve independent microrobot control and implement the microassembly scheme.

Our control scheme minimizes the control voltage bandwidth requirements of an n-microrobotic system. The sub-linear ($O(\sqrt{n})$) control voltage bandwith requirement is a large improvement over $O(n)$ in our previously proposed approach [6]. Reducing the control voltage bandwidth requirement was the enabling technology that allowed us to experimentally demonstrate simultaneous control of four devices. We used the STRING control matrix to implement planning and control algorithms that reduce parallel motion of n robots to parallel motion of only two robots, followed by sequential motion of single devices. Our algorithms are not completely general, however, they allowed efficient control of stress-engineered microrobotic systems with sufficient free space. We used the theory of EDR to extend our planning algorithms to correct for control error, which would otherwise accumulate unacceptably during the operation of our microrobots. The work presented in this paper attacks the control of stress-engineered multi-microrobotic systems by selectively addressing the behavior of individual devices through a common control signal. We believe this concept of selective response to a global control signal (GCSR [5]) will be important for controlling future multi-microrobotic systems. GCSR is common in biological, micro, and nano-scale systems, and may be the paradigm of choice for controlling groups of micro, and nano-robots.

Acknowledgements

This work was supported by grant number GM-65982 to B.R.D. from NIH, and 2000-DT-CX-K001 to B.R.D., from the Office for Domestic Preparedness, Department of Homeland Security, USA. The electron micrographs were taken at the Dartmouth Ripple Electron Microscopy Laboratory, with the help of C. P. Daghlian. We thank U. J. Gibson for the use of equipment in her lab, and for many helpful discussions. We further thank D. Balkcom, C. Bailey-Kellogg, A. Lebeck and K. Böhringer for their advice and suggestions.

References

1. K.-F. Böhringer, B. R. Donald, R. R. Mihailovich, and N. C. MacDonald. A theory of manipulation and control for microfabricated actuator arrays. In *the Proceedings of the IEEE Workshop on Micro Electro Mechanical Systems MEMS*, January 1994.
2. T. Bretl. Control of many agents using few instructions. In *the Proceedings of Robotics: Science and Systems 2007 conference*, Atlanta, GA, 2007.

3. N. Dechev, W. L. Cleghorn, and J. K. Mills. Tether and joint design for micro-components used in microassembly of 3D microstructures. In *in the proceedings of SPIE Micromachining and Microfabrication, Photonics West 2004*, January 2004.
4. B. R. Donald. *Error Detection and Recovery in Robotics. Lecture Notes in Computer Science*, volume 336. Springer-Verlag, 1987.
5. B. R. Donald. Building very small mobile micro robots. Inaugural Lecture, Nanotechnology Public Lecture Series, MIT (Research Laboratory for Electronics, EECS, and Microsystems Technology, Laboratories). Cambridge, MA., April 2007. avaliable online at: http://mitworld.mit.edu/video/463/.
6. B. R. Donald, C. G. Levey, C. McGray, I. Paprotny, and D. Rus. An untethered, electrostatic, globally-controllable MEMS micro-robot. *Journal of Microelectromechanical Systems*, 15(1):1–15, January 2006.
7. B. R. Donald, C. G. Levey, C. McGray, D. Rus, and M. Sinclair. Power delivery and locomotion of untethered micro-actuators. *Journal of Microelectromechanical Systems*, 10(6):947–959, December 2003.
8. B. R. Donald, C. G. Levey, and I. Paprotny. Planar microassembly by parallel actuation of MEMS microrobots. *Journal of Microelectromechanical Systems*, 17(4):789–808, August 2008.
9. B. R. Donald, C. G. Levey, and I. Paprotny. Planar microassembly by parallel actuation of MEMS microrobots – supplementary videos (2008). [Online]. Avaliable: www.cs.duke.edu/donaldlab/Supplementary/jmems08/, 2008.
10. B. R. Donald, C. G. Levey, I. Paprotny, and D. Rus. Simultaneous control of multiple MEMS microrobots – supplementary material. Department of Computer Science, Duke University, July 2008. [Online]. Avaliable: http://www.cs.duke.edu/donaldlab/Supplementary/wafr08/.
11. S. Hollar, A. Flynn, C. Bellew, and K. S. J. Pister. Solar powered 10 mg silicon robot. In *the proceedings of the The Sixteenth Annual International Conference on Micro Electro Mechanical Systems, 2003. MEMS-03 Kyoto.*, pages 706–711, Kyoto, Japan, Januar 19th-23rd, 2003.
12. L. Jianghao, L. Zhenbo, and C. Jiapin. An omni-directional mobile millimeter-sized microrobot with 3-mm electromagnetic micromotors for a micro-factory. *Advanced Robotics*, 21(12), December 2007.
13. D. Popa and H. E. Stephanou. Micro and meso scale robotic assembly. *SME Journal of Manufacturing Processes*, 6(1):52–71, 2004.
14. J. W. Suh, R. B. Daring, K. F. Bohringer, B. R. Donald, H. Baltes, and G. T. A. Kovacs. CMOS integrated ciliary actuator array as a general-purpose micromanipulation tool for small objects. *Journal of Microelectromechanical Systems*, 8(4):483–496, December 1999.
15. G. M. Whitesides and B. Grzybowski. Self-assembly at all scales. *Science*, 295:2418–2421, March 2002.
16. K. B. Yesin, K. Vollmers, and B. J. Nelson. Modeling and control of untethered boimicrorobots in fluid environment using electromagnetic fields. *The International Journal of Robotics Research*, 25(5-6):527–536, May-June 2006.